PSFC/JA-07-2

Equilibrium beta limits in a dipole configuration

Luca Guazzotto, Jeffrey P. Freidberg and Jay Kesner

MIT Plasma Science and Fusion Center,
167 Albany Street, Cambridge, MA 02139, U.S.A.

Equilibrium limits in a dipole configuration

L. Guazzotto   J. P. Freidberg   J. Kesner

Massachusetts Institute of Technology, Plasma Science and
Fusion Center, Cambridge, Massachusetts 02139

Abstract

The levitated dipole configuration is an innovative concept for fusion research. One of the main advantages of the dipole configuration is the possibility of stably confining high plasma pressure compared to the magnetic pressure, that is the possibility of achieving high βs (where β is the ratio between plasma pressure and magnetic pressure). The present work investigates the limit on equilibrium β existing in the dipole system. It is found that a limit exists, which is considerably modified by the presence of plasma rotation in the toroidal direction (the long way around the torus). Plasma anisotropy instead does not modify the limit in any appreciable way for the moderate anisotropies considered in this work.

I. Introduction

One important measure of attractiveness of the levitated dipole configuration for fusion energy applications is its MHD β limit. A high stable value is required because of the need to use advances fuel cycles, such as D-D (deuterium-deuterium) to avoid an excessive neutron wall loading on the surface of the superconducting levitating coil. [1]

The issue has been addressed by the means of a cylindrical analysis in which the Levitated Dipole Experiment (LDX) is modeled by a linear, hard core Z-pinch [2]. The result shows that MHD sets three β limits (where β is the ratio between thermal and magnetic pressure). The first is a pure equilibrium limit arising from the need to keep the pressure hollow with a zero value at the surface of the levitation coil. This limit for the cylindrical model (with the ratio of specific heats $\gamma = 2$) is quite high: $\bar{\beta} \leq 0.84$. Here $\bar{\beta}$ is the volume averaged "beta" defined such that $0 \leq \bar{\beta} \leq 1$. The second limit is due to the $m = 1$ helical mode. [2] Here, the hard core provides a strong stabilizing effect leading to the limit $\bar{\beta} \leq 0.54$, again a reasonably high value. The third and strictest limit arises from the $m = 0$ interchange mode [3] (i.e. the sausage instability). This mode is stabilized when the pressure profile decreases sufficiently gradually near the outer edge of the plasma and the result is a limit $\bar{\beta} \leq 0.5$. All limits have been obtained with a specific, but realistic, shape for the plasma pressure profile. The conclusion from the cylindrical analysis is that the MHD β limits are all high, a desirable result for LDX.

Still, some caution should be exercised since LDX is a toroidal con-

figuration with a tight aspect ratio. Thus, while the cylindrical results provide good qualitative insight, the analysis should be repeated for the more realistic toroidal geometry to obtain more reliable quantitative predictions. In the present work we address the first and simplest of the MHD β limits, that due purely to equilibrium force balance.

Since the configuration of interest corresponds to a 2-D axisymmetric torus the results must be obtained numerically. This is accomplished by means of the MHD equilibrium code FLOW [5], which solves a generalized form of the Grad-Shafranov (GS) equation, including the effects of toroidal flow and pressure anisotropy as well as the usual pressure gradient and magnetic forces.

The results show that for the isotropic case with zero flow the equilibrium β limit persists. The actual β limit is substantially lower that for the cylindrical case because of the large volume of low pressure plasma that arises in the outer region of the dipole magnetic configuration. For the studies presented here we find that the equilibrium β limit is reduced to $\bar{\beta} \leq 0.046$. This result has also been obtained for a specific, but reasonable, shape of the pressure profile. In particular, we consider only profiles with a single peak in the plasma region corresponding to a single frequency external electron cyclotron heating.

The next set of numerical calculations adds the effect of toroidal rotation, keeping the plasma isotropic. Flow reduces the β limit since the confining magnetic field must now be apportioned between both the thermal and centrifugal forces. The amount of $\bar{\beta}$ reduction depends upon the magnitude of the flow and how close its peak is with

3

respect to the pressure peak. The largest reduction occurs when the peaks overlap. For this case a flow corresponding to a sonic Mach number $M_\varphi = 0.4$ reduces the $\bar{\beta}$ limit to about 77% of the static value. Here $M_\varphi^2 = \left(V_\varphi^2\right)_{max} / \left(\gamma p / \rho\right)_{max}$.

The last set of numerical studies includes the effect of pressure anisotropy but sets the flow to zero. The interesting experimental case, corresponding to electron cyclotron heating, has $p_\perp > p_\parallel$. The results show that for reasonable experimental ratios, $p_\perp / p_\parallel \lesssim 1.4$, anisotropy makes only a small correction to the equilibrium β limit.

The main part of the paper describes these results in detail in the following order: (1) review of the cylindrical results, (2) formulation of the toroidal equilibrium problem, (3) $\bar{\beta}$ limits for an isotropic plasma with zero flow, (4) $\bar{\beta}$ limits for an isotropic plasma with non-zero flow, and (5) $\bar{\beta}$ limits for an anisotropic plasma with zero flow.

II.   The cylindrical model

A basic understanding of the equilibrium limit in a dipole configuration can be obtained utilizing a cylindrical model, and this is the goal of the present section. By ignoring toroidal curvature and non-circularity, one can model a levitated dipole system by a hard core Z-pinch; the hard core corresponds to the levitating dipole coil. In the absence of an axial magnetic field, in a cylinder the equilibrium is described by the familiar relation:

$$\frac{dp}{dr} + \frac{B_\theta}{\mu_0 r} \frac{d}{dr}(r B_\theta) = 0, \tag{1}$$

4

where p is the plasma pressure, r the radial coordinate, μ_0 the permeability of free space and B_θ the poloidal component of the magnetic field. A physical pressure profile has vanishing $p(r)$ on the surface of the coil and as $r \to \infty$. The pressure peaks at an intermediate value of r. Furthermore, for a cylinder interchange stability requires the pressure profile to satisfy

$$-\frac{rp'}{p} \leq \frac{2\gamma B_\theta^2}{B_\theta^2 + \mu_0\gamma p} \approx 2\gamma, \tag{2}$$

the simplified form being valid in the region of low plasma pressure. In a torus, the simplified form of the stability criterion can be written as

$$-\frac{d}{d\psi}\left(pV^\gamma\right) \leq 0, \tag{3}$$

where $V(\psi)$ is the volume of the flux tube and γ the adiabatic index.

A cylindrical pressure profile satisfying the previous requirements is given by: [2]

$$p(r) = K\frac{r^2 - r_1^2}{(r^2 + r_1^2)^{\gamma+1}} \tag{4}$$

where K is a constant determining the magnitude of the pressure and r_1 is the hard core (coil) radius. If one chooses $\gamma = 2$, then an exact solution to equation (1) can be found:

$$B_\theta = \frac{\mu_0(I_c + I_p)}{2\pi r}\sqrt{1 - 8\bar{\beta}\frac{(r/r_1)^4}{[1 + (r/r_1)^2]^3}}, \tag{5}$$

with

$$\bar{\beta} = \frac{16\pi^2}{\mu_0(I_c + I_p)^2}\int_{r_1}^{\infty} pr\mathrm{d}r = 1 - \left(\frac{I_c}{I_c + I_p}\right)^2 \tag{6}$$

and where I_c and I_p are the coil and plasma current, respectively. Note that with this definition $0 \leq \bar{\beta} < 1$. Pressure and poloidal field

5

profiles for a high-$\bar{\beta}$ equilibrium are illustrated in Fig. 1 in arbitrary units. The pressure profile is assigned by equation (4), where $K = [\mu_0(I_c + I_p)^2 r_1^4/2\pi^2]\bar{\beta}$. Note that $\bar{\beta}$ enters in the definition of the pressure profile only as a multiplicative constant. The poloidal field profile is determined as function of $\bar{\beta}$ by equation (5). It is clear from equation (5) that as $\bar{\beta}$ increases B_θ decreases. The "dip" in B_θ appearing as effect of high plasma pressure is easily recognizable in Fig. 1. Eventually, when $\bar{\beta}$ is sufficiently large $B_{\theta min}$ vanishes at $r = \sqrt{2}r_1$. This is the equilibrium $\bar{\beta}$ limit. The plasma has expelled all of the magnetic field from the high pressure region and further increases in $\bar{\beta}$ cannot be confined. An alternate interpretation is that in order to satisfy the requirement $p(r_1) = 0$, the current in the hard core is only capable of maintaining the hollow pressure profile for values of $p(r) \le p_{max}$, where p_{max} corresponds to the equilibrium limit.

For the particular choice of $\gamma = 2$, the equilibrium limit, which is quite high, is $\bar{\beta} = 27/32 \simeq 0.84$. The analytical solution has been used to benchmark the equilibrium code FLOW [5], which has been used for all equilibrium calculations described in the remainder of this work. If a more realistic value of $\gamma = 5/3$ is chosen, equation (1) must be solved numerically; the numerical solution gives a $\bar{\beta}$ limit of $\bar{\beta} \simeq 0.89$.

The same physics described here applies to a toroidal plasma: as $\bar{\beta}$ is increased, the poloidal field becomes more and more hollow, until it vanishes at a critical value of $\bar{\beta}$. The discussion of the toroidal system

is introduced in the next section.

III.   Equilibrium $\bar{\beta}$ limit in a toroidal geometry

The LDX equilibrium is characterized by an axisymmetric toroidal geometry with non-circular cross section and $B_\varphi = 0$. Therefore, it is described by a Grad-Shafranov (GS) equation. In the analysis, the effects of toroidal flow and anisotropy are also included, leading to a modified GS equation, given by Ref. [4]. The details of the formulation are described in references [4] and [5]. In the present section we will only state the results needed for the discussion in the rest of this work. The three versions of the Grad-Shafranov equation used in the analysis are as follows:

isotropic, no flow:

$$\frac{1}{\mu_0} \nabla \cdot \left(\frac{\nabla \psi}{R^2} \right) = -\frac{dp(\psi)}{d\psi} \tag{7a}$$

isotropic, with flow:

$$\frac{1}{\mu_0} \nabla \cdot \left(\frac{\nabla \psi}{R^2} \right) = -\rho \frac{R^2 - R_0^2}{2} \frac{d\Omega^2}{d\psi} - \frac{\gamma \rho}{\gamma - 1} \frac{d}{d\psi} \left(\frac{P}{D} \right) + \frac{\rho^\gamma}{\gamma - 1} \frac{d}{d\psi} \left(\frac{P}{D^\gamma} \right) \tag{7b}$$

anisotropic, no flow:

$$\frac{1}{\mu_0} \nabla \cdot \left[(1 - \Delta) \left(\frac{\nabla \psi}{R^2} \right) \right] = -\rho \frac{dT_\parallel(\psi)}{d\psi} \tag{7c}$$

7

In each of these equations the poloidal flux is defined in the standard way:

$$\boldsymbol{B} = \frac{\nabla \psi \times \boldsymbol{e}_\varphi}{R}. \qquad (8)$$

For the first case [Eq. (7a)], corresponding to an isotropic plasma with zero flow, there is a single free function, the pressure $p = p(\psi)$.

For the second case [Eq. (7b)], the plasma remains isotropic, but has a toroidal flow $v_\varphi = R\Omega(\psi)$. In this situation there are three free functions, the angular velocity $\Omega(\psi)$, the "quasi-pressure" $P(\psi)$ and the "quasi-density" $D(\psi)$. Notice that neither the pressure nor the density are flux functions; more details about the relation between the two physical quantities and their corresponding quasi-functions are given in Ref. [5]. Here we will just state the results:

$$\rho = D \left[1 + \frac{1}{2}(R^2 - R_0^2)\Omega^2 \frac{\gamma - 1}{\gamma} \frac{D}{P} \right]^{\frac{1}{\gamma - 1}}, \qquad (9)$$

$$p = P \left[1 + \frac{1}{2}(R^2 - R_0^2)\Omega^2 \frac{\gamma - 1}{\gamma} \frac{D}{P} \right]^{\frac{\gamma}{\gamma - 1}}, \qquad (10)$$

which are obtained by solving the Bernoulli equation, i.e. the $\boldsymbol{B}$ component of the momentum equation. In the following calculations, the value $\gamma = 5/3$ has been used.

The final case of interest [Eq. (7c)] includes the effect of pressure anisotropy, but assumes zero flow. The anisotropy enters in the left hand side of Eq. (7c) as:

$$\Delta \equiv \frac{p_\parallel - p_\perp}{\mu_0 B^2} \qquad (11)$$

For this case there are four free functions, $T_\parallel(\psi)$, $\Theta(\psi)$, $D(\psi)$ and $B_0(\psi)$. Due to the high thermal conductivity along the field lines,

thermal equilibration along the field lines is assumed to occur on time scales much faster than any other equilibration time in the system. That requires the plasma temperature along the field lines to be a flux function, $T_{\parallel} = T_{\parallel}(\psi)$. The other free functions enter through the density:

$$\rho = D\frac{B}{B_0}\left|\frac{B_0 - \Theta T_{\parallel}}{B - \Theta T_{\parallel}}\right|. \tag{12}$$

The quasi-density $D(\psi)$ maintains the same meaning as in the case of Eq. (7b). The anisotropy is defined through $\Theta(\psi)$:

$$T_{\perp} \approx T_{\parallel}(\psi)\frac{B}{B - \Theta(\psi)T_{\parallel}(\psi)}. \tag{13}$$

Pressures and temperatures are connected by two equations of state, $p_{\parallel,\perp} = \rho T_{\parallel,\perp}$. Finally, $B_0(\psi)$ is an integration constant with the dimensions of a magnetic field.

An ideal gas relation is used to close the system also in the isotropic case, writing $p = \rho T$. In the isotropic case temperature has been eliminated from equations (7), (9) and (10) through the ideal gas relation.

The equilibrium code FLOW [5] is used to solve equation (7). The code was originally developed for the study of tokamak equilibria in the presence of macroscopic flow. In order to apply the code to the dipole equilibrium problem, a few modifications have been required, namely:

1. An inner boundary condition is introduced to model the dipole coil.

2. A non-uniform mesh is required since the flux surfaces are far

9

from concentric with respect to the inner and outer edges of the plasma. The non-uniform grid provides high resolution near the levitation coil. The grid is coarser in the far outboard region, where plasma pressure is low and lower accuracy is necessary.

3. Since the grid is non-uniform, the finite-difference differential operators used for the numerical solution of equation (7) need to be modified to retain second order accuracy (with respect to the grid step).

In the present work FLOW is used to solve Eq. (7) in the customary "fixed-boundary" mode. Here the inner and outer plasma contours are given as part of the input and information related to ψ is specified on each surface. Different approximations have been considered for the boundary shape and boundary conditions. In the present section, we only discuss the approximation that has been used in the remainder of this work.

The outer boundary is chosen as a vacuum flux surface located in close proximity to the actual LDX chamber wall, arising from a simple dipole current located on the centroid, $R = R_0$, $Z = 0$, of the actual LDX coil current. The geometry is represented in Fig. 2. Specifically, the outer surface $r_0(\theta)$ is evaluated by numerically inverting:

$$\psi_V(r_o, \theta) = \psi_V(R_w - R_0, 0), \tag{14}$$

where R_w is the midplane wall radius and ψ_V is the vacuum flux due to the circular current filament.

In a similar way, the inner boundary is also assigned as a vacuum

flux surface. The inner surface has an inner radius $r_i(\theta)$, which is determined by modeling the LDX coil with a set of $N = 1906$ circular filaments. The vacuum flux surfaces are then determined by simple superposition. The geometry of the inner boundary and of the LDX magnet is schematically represented in Fig. 3. The inner radius r_i is determined by requiring the the inner magnetic surface be tangent to the actual surface of the levitation coil. For simplicity, the surface is held fixed as β is increased.

Having specified the boundary shapes, the next step is to specify the boundary conditions. Since each boundary is assumed to be a flux surface, the appropriate boundary conditions are:

$$\psi[r_0(\theta), \theta] = \psi_o = const. \tag{15a}$$

$$\psi[r_i(\theta), \theta] = \psi_i = const. \tag{15b}$$

Varying the value of $\psi_i - \psi_o$ is equivalent to varying the value of β, as discussed in more detail in section IV. One of these parameters (e.g. ψ_i) can be set arbitrarily, and is kept fixed at the vacuum value.

In order to calculate the equilibrium β limit, it is now necessary to choose a meaningful definition of β. Intuitively, the local $\beta = 2\mu_0 p(\boldsymbol{r})/B(\boldsymbol{r})^2$ is not a convenient definition for the present problem. The reason is that the local β always diverges at the equilibrium limit, since the magnetic field vanishes. Therefore, the local β contains no information about the total amount of plasma pressure that can be confined before reaching the equilibrium limit. A more meaningful definition is global in nature, similar to the definition for the

11

cylindrical case of equation (6):

$$\bar{\beta} = 2\mu_0 \frac{\bar{p}}{\bar{B}^2},$$ (16)

with

$$\bar{p} = \frac{1}{V} \int p \mathrm{d}\mathbf{r}, \qquad \bar{B} = \frac{1}{L} \oint B \mathrm{d}\ell.$$ (17)

Note that the volume integral is computed over the plasma volume, while the line integral is evaluated over the outer plasma boundary $r = r_0(\theta)$. Also, V is the plasma volume, and L is the poloidal perimeter of the outer boundary surface. The global β is indicated with the symbol $\bar{\beta}$ to distinguish it from the local β.

We observe that different definitions of a global β (e.g. ratio between plasma stored energy and field stored energy) are possible and used in the literature. A different definition of β would produce different numerical values, but maintain the same general behavior of the equilibrium limit. Our choice, expressed by Eq. (16) is motivated by the fact that Eq. (16) is the natural extension to a toroidal system of the cylindrical definition in Eq. (6).

Equilibrium $\bar{\beta}$ limit results are discussed in the next sections.

IV.   Equilibrium $\bar{\beta}$ limits for a static plasma

The procedure for determining equilibrium limits in an isotropic plasma with zero flow [modeled by Eq. (7a)] is as follows. The first step consists of choosing a plausible profile for $p(\psi)$, which must vanish on the

inner tangent surface $\psi = \psi_i$ and decay sufficiently gradually in the outer low pressure region such that $pV^\gamma \to const$.

Implementation of the outer constraint requires a knowledge of the relationship between V and ψ. This result is ascertained by noting that in this region the field is accurately approximated by a vacuum field. A simple analytic estimate, supported by a straightforward numerical calculation shows that for a vacuum field $V \approx K/\psi^4$ as $\psi \to 0$ for large R (using our normalization constant for the flux).

An additional experimental constraint is given by the plasma pressure on the wall, which is set by its material properties. It cannot be too large, or else the thermal load on the wall and the energy losses of the plasma are too large.

Combining these constraints leads to the following plausible choice for $p(\psi)$:

$$p(\psi) = p_0 \left(1 - \frac{\psi}{\psi_i} \right)^2 \left(\frac{\psi}{\psi_i} \right)^{4\gamma}. \tag{18}$$

The value p_0 is a derived quantity obtained as follows:

$$p_0 = \frac{p_w}{\left(\frac{\psi_o}{\psi_i} \right)^{4\gamma} \left(1 - \frac{\psi_o}{\psi_i} \right)^2}. \tag{19}$$

The value $p_w = 12 \, [Pa]$ is a typical acceptable wall pressure and is a fixed input for all the numerical simulations. This leaves ψ_o as the only free quantity, which controls the value of p_0 and therefore β. It is intuitive from equation (19) that when $\psi_o \to 0$ the value of $p_0 \to \infty$ implying that $\beta \to \infty$. The numerical problem of determining the equilibrium limit thus reduces to the problem of finding the minimum ψ_o for which the equilibrium solution exists.

13

The equilibrium $\bar{\beta}$ limit is determined by running FLOW with the same profile for the input $p(\psi)$, but increasing the constant p_0 in equation (18) by decreasing ψ_o until the poloidal field value inside the field "dip" approaches 0. The equilibrium limit is defined by the value of p_0 for which the minimum of the field is exactly 0. In practice, because of numerical limitations the equilibrium limit is determined by the value of p_0 (and hence $\bar{\beta}$) for which the minimum field is $\lesssim 0.1\%$ of the field on the outboard side of the coil along the midplane.

The results of a typical set of calculations for the equilibrium limit for a static plasma with the pressure profile given by Eq. (18) are illustrated in Fig. 4, which shows the magnetic field profile along the midplane in the outer part of the plasma (outboard side of the coil) for different values of $\bar{\beta}$. It is clear that as the pressure increases the field minimum becomes smaller, until the equilibrium limit is reached for a value of $\bar{\beta} \simeq 4.6\%$.

Observe that the $\bar{\beta}$ limit is much lower than for the cylindrical case (i.e. $\bar{\beta} = 0.89$). There are two reasons for such a considerable difference. The first is associated with the pressure profile. Because of the effect of toroidal geometry on the dependence of $V(\psi)$ on ψ (i.e. $V \propto 1/\psi^4$), the pressure profile decays much more rapidly for large R in the toroidal case. Second, there is a large penalty on the value of $\bar{\beta}$ due to the geometry, since the low-pressure regions have a larger weight in the average than they would in the cylindrical case. The $\bar{\beta}$ limit can be increased by changing the pressure profile, in particular by generalizing the factor $(1 - \psi/\psi_i)^2 \rightarrow (1 - \psi/\psi_i)^\alpha$ and choosing $\alpha > 2$.

14

Even so the overall increase in $\bar{\beta}$ is not too large and the original conclusions remain valid. The value $\alpha = 2$ is used in the calculations as this produces a pressure maximum at $R \approx 0.7m$, which is consistent with the experimental operation of LDX.

The overall conclusion is that an equilibrium $\bar{\beta}$ limit exists in a torus which is qualitatively similar to that in a cylinder. However, quantitatively the toroidal $\bar{\beta}$ limit is much smaller, by an order of magnitude, because of toroidal geometric effects.

The effect of toroidal rotation is considered next.

V.   Equilibrium limits in the presence of toroidal flow

Many fusion experiments exhibit a substantial toroidal flow velocity. Sometimes these flows are externally driven, for instance by neutral beams. Often times the flows arise spontaneously with, at present, no first principles explanation. In any event, the likely presence of a toroidal flow in LDX may lead to a significant reduction in the equilibrium $\bar{\beta}$ limit. The reason is that a given poloidal magnetic field must confine both the particle pressure gradient force and the centrifugal force. Thus, a smaller fraction of the magnetic field is available to provide pressure balance and this leads to a reduction in the $\bar{\beta}$ limit.

The effect of toroidal flow on the $\bar{\beta}$ limit in LDX is the subject of this section. The approach taken is to start with a static equilib-

rium as described in the previous section and then slowly increase the flow velocity until the equilibrium limit is reached. Specifically, the starting static profile corresponds to a plasma pressure equivalent to $\bar{\beta} = 0.43\bar{\beta}_{max}$ where $\bar{\beta}_{max} = 0.046$ is the static limit. The aim of the calculation is to determine how large the flow velocity must become to reach the equilibrium limit; that is, we want to calculate $M_\varphi = m_\varphi(\bar{\beta})$ for $\bar{\beta} = 0.43\bar{\beta}_{max}$ where $M_\varphi = \left[\Omega R/(\gamma p/\rho)^{1/2}\right]_{max}$ is the maximum value of the thermal Mach number along the mid-plane $Z = 0$. The simulations are carried with the following choices for the free functions. The quasi pressure is given by its static form $P(\Psi) = p_{static}(\Psi)$ in Eq. (18). For simplicity, the quasi density function is chosen as a simple power law expression:

$$D(\psi) = D_w + (D_{max} - D_w)\sqrt{\frac{\psi - \psi_o}{\psi_i - \psi_o}}. \qquad (20)$$

Here, the density is a monotonically decreasing function of distance away from the levitation coil with D_{max} representing the coil density and D_w representing the outer wall density. Simulations using various density profiles, but holding D_{max}, D_w fixed indicate only a weak sensitivity to the profile shape.

Two choices are used for the flow velocity profile. These are illustrated in Fig. 5. The first profile (solid curve) is peaked near the pressure maximum. The second profile (dashed curve) is peaked well beyond the pressure maximum. The results of the simulations are as follows.

For the first velocity profile, curves of $|B|$ vs. R are illustrated in Fig. 6 for various values of M_φ. Note that as the velocity increases,

the minimum value of $|B|$ decreases. We see that when the pressure and velocity peak near the same radius, a modest value of Mach number, $M_\varphi \approx 0.4$, is sufficient to reach the equilibrium limit. At the limit we find $\bar{\beta} = 0.77\bar{\beta}_{max}$ (and not $\bar{\beta} = 0.43\bar{\beta}_{max}$). The reason for this difference is that it is the quasi pressure function $P(\Psi)$ that is held fixed as the rotation is increased. The actual pressure is not a flux function when the flow is non-zero, and thus the value of $\bar{\beta}$ can and does change as the flow velocity is increased. The net result is that modest flow velocities peaked near the pressure maximum can lead to substantial reductions in the equilibrium $\bar{\beta}$ limit.

Consider now the second velocity profile. The simulations show that much higher peak flow velocities can be achieved without reaching the equilibrium limit. The reason is that the full magnetic field is effectively available to confine both the pressure gradient force and the centrifugal force since they peak at very different locations. There is no need to apportion the field at a single location as is required when the peaks overlap. Curves of $|B|$ vs. R are illustrated in Fig. 7 for a high flow and a static equilibrium for the case where $\bar{\beta} = 0.43\bar{\beta}_{max}$ for no flow. Observe that the solid curve has not yet reached the equilibrium limit even though its corresponding $M_\varphi \approx 1.5$, a much higher value than is possible when the peaks overlap. The conclusion is that a velocity profile peaked far from the pressure peak is capable of driving the system to its equilibrium limit, although very high values of M_φ would be required to do so.

As a final comment to this section, it is concluded that very high

rotations could in principle take the LDX plasma to an equilibrium limit. More importantly, even slower rotations can have a significant effect on the equilibrium limit, if they are localized close to the pressure peak. For that reason, determining the rotation profile will be of considerable importance for the experimental operation of LDX, if the plasma pressure is increased to values of the order of the static equilibrium limit.

VI.   The effect of pressure anisotropy

The LDX experiment is heated by electron cyclotron waves. Such waves preferentially provide heat to the perpendicular particle pressure, thereby producing an anisotropic plasma. The effect is particularly pronounced in the early LDX experiments where the levitation coil is actually held in place by mechanical supports. The resulting plasma density is low which limits the ability of Coulomb collisions to isotropize the pressure. Even when the coil is levitated, there is still likely to be a substantial anisotropy, since the heating will still occur in an anisotropic fashion. The anisotropy level will depend on the ratio between the pitch angle scatter time and the particle confinement time.

The brief discussion just presented motivates the simulations described in this section which attempt to determine the effects of anisotropy on the equilibrium $\bar{\beta}$ limit. The simulations assume a zero toroidal flow velocity and an anisotropy characterized by $p_\perp > p_\parallel$. The free

functions chosen for the simulations are given by:

$$T_{\parallel}(\Psi) = m_i p_0(\Psi)/D(\Psi),$$

$$D(\psi) = D_w + (D_{max} - D_w)\sqrt{\frac{\psi - \psi_o}{\psi_i - \psi_o}},$$

$$B_0(\Psi) = \hat{B}_0 = const.,$$

$$\Theta(\Psi) = \Theta_0 exp\left[-\alpha_\Theta \left(\frac{\Psi - \Psi_{max}}{\bar{\Psi}}\right)^2\right],$$

(21)

where $p_0(\Psi)$ is the static, isotropic pressure profile, given by Eq. (18), Ψ_{max} is the value of Ψ for which $p_0(\Psi)$ is maximum, and $\bar{\Psi}$ is defined as $max(|\Psi_{max} - \Psi_i|, |\Psi_{max} - \Psi_o|)$. Note that in the isotropic limit $\Theta = 0$, the pressure reduces to

$$p(\Psi) = T_{\parallel}(\Psi)D(\Psi)/m_i = p_0(\Psi),$$

(22)

the standard form given by Eq. (18) (m_i is the ion mass). A slightly subtle point needs to be considered in the definition of the free function $\Theta(\Psi)$. For the ratio $T_\perp/T_\parallel$ to remain finite near the equilibrium limit, the function $\Theta(\Psi)$ must approach zero at least at the same rate that $B(R, Z)$ approaches zero. See Eq. (13). The requirement can be satisfied in different ways, but we find expedient to assign $\Theta(\Psi)$ to be effectively zero everywhere (and in particular near the minimum of $|B|$) except around the pressure maximum. That is obtained through the exponential decay in Eq. (21), assigning $\alpha_\Theta = 20$. The level of anisotropy is varied by choosing different values for Θ_0.

The simulations are carried out as follows. The starting point is a reference case corresponding to isotropic pressure (i.e. $p = p_0(\Psi)$, $\Theta = 0$). Anisotropy is introduced in a series of equilibria by slowly

increasing the magnitude of Θ_0. For these simulations the free functions $T_\parallel(\Psi)$, $D(\Psi)$, and $B_0(\Psi)$ are held fixed. This choice leaves the parallel pressure essentially unchanged as the anisotropy is increased. It is not exactly unchanged since it is $D(\Psi)$ that is fixed and not the density ρ, which is not a flux function in the presence of anisotropy, as expressed by Eq. (12). For each equilibrium the value of $\bar{\beta}$, defined as $\bar{\beta} = \left(\bar{\beta}_\parallel + 2\bar{\beta}_\perp\right)/3$, is calculated along with the corresponding value of $|B_{min}|$. A fair comparison with the isotropic case is made as follows. For the isotropic case the amplitude of the pressure $p_0(\Psi)$ is rescaled and the solution recomputed so that the resulting isotropic value of $\bar{\beta}$ is identical to the anisotropic value. Also, the new rescaled value of $|B_{min}|$ is recalculated.

The effects of anisotropy can then be determined by comparing the values of B_{min} as a function of Θ_0 at fixed $\bar{\beta}$. The lower the value of B_{min} the closer the configuration is to the equilibrium limit. Two curves of $|B|$ vs. R for an isotropic and an anisotropic equilibrium with $\bar{\beta} = 0.43\bar{\beta}_{max}$ are shown in Fig. 8. Note that anisotropy raises B_{min}, and therefore the critical equilibrium $\bar{\beta}$ limit. However, even for substantial anisotropy $((p_\perp/p_\parallel)_{max} \approx 1.44)$, the change in B_{min} is small implying only a small change in the actual equilibrium $\bar{\beta}$ limit.

VII. Conclusions

The equilibrium pressure limits of a dipole configuration, with particular emphasis on the Levitated Dipole Experiment LDX, have been

examined in the present work. The equilibrium limit is reached when the plasma pressure becomes so large in a region of the plasma that it completely expels the magnetic field, leading to a loss of confinement. An isotropic, static plasma was considered first, showing that for realistic pressure profiles the equilibrium limit is reached for values of $\bar{\beta}$ of approximately 4.6%, where $\bar{\beta}$ is the ratio between the average plasma and magnetic pressure defined in equation (16). Toroidal rotation, which could play a role in LDX experiments, has been showed to substantially affect the equilibrium limit if the rotation is peaked in the proximity of the pressure peak. For such profiles, even strongly subsonic flows ($M_\varphi \simeq 0.4$) considerably reduce the equilibrium limit. On the other hand, a rotation on the order of the plasma sound speed is necessary in order to influence the equilibrium limit in the same measure if the flow is localized away from the pressure peak. Lastly, due to the heating mechanism in LDX, some anisotropy could also be present in the equilibrium, but that does not seem to affect the equilibrium limit in the range of anisotropies examined in this work.

All the results presented in this work have been obtained assuming a specific pressure profile, with a single peak. Different profiles with a single peak would produce different numerical results, but similar physics. The effect of multiple pressure peaks in the equilibrium will be considered in future work.

In conclusion, we have demonstrated the existence of an equilibrium pressure limit for a dipole configuration, which significantly constrains the maximum amount of plasma pressure that can be confined.

21

VIII. Acknowledgments

References

[1] J. Kesner, D. T. Garnier, A. Hansen, M. Mauel, L. Bromberg, Nucl. Fusion **44**, 193 (2004)

[2] J. P. Freidberg, Plasma Physics and Fusion Energy, Cambridge University Press, *in press*

[3] A. N. Simakov, P. J. Catto, S. I. Krasheninnikov, J. J. Ramos, Phys. Plasmas **7**, 2526 (2000)

[4] R. Iacono, A. Bondeson, F. Troyon and R. Gruber, Phys. Fluids B **2**, 1794 (1990)

[5] L. Guazzotto, R. Betti, J. Manickam and S. Kaye, Phys. Plasmas **11**, 604 (2004)

[6] J. A. Stratton, Electromagnetic Theory (McGraw-Hill, New York 1941) pag. 263

[7] D. T. Garnier, J. Kesner and M. E. Mauel, Phys. Plasmas **6**, 3431 (1999)

List of Figures

Figure 1: Pressure and poloidal field in the cylindrical case (plot in arbitrary units).
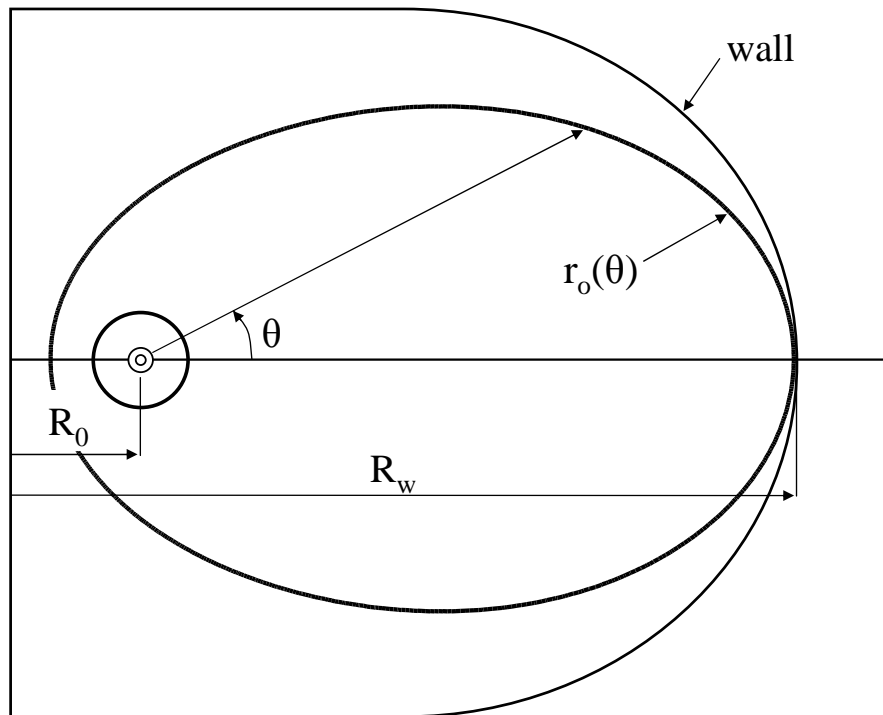
Figure 2: LDX calculation boundary schematic representation.
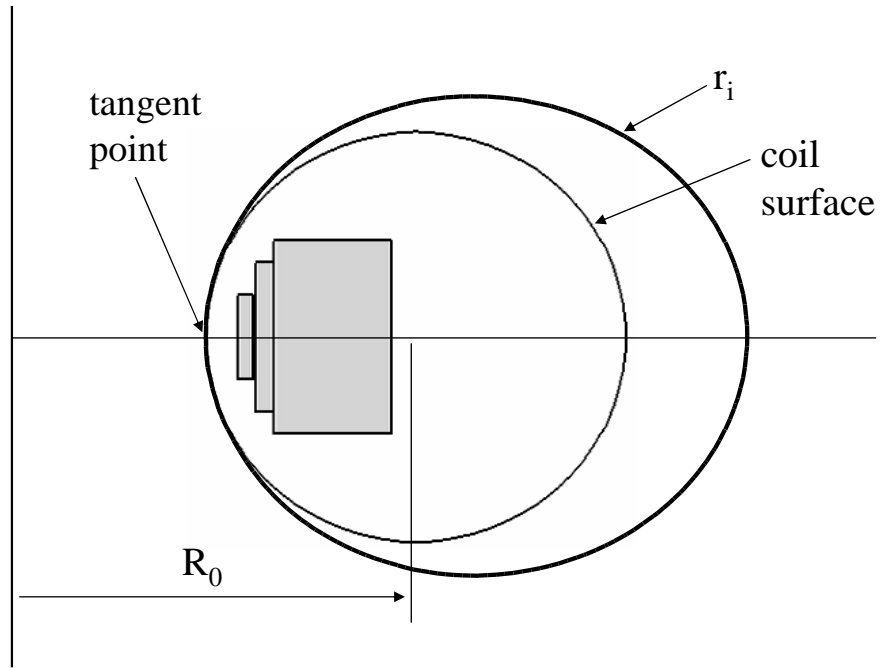
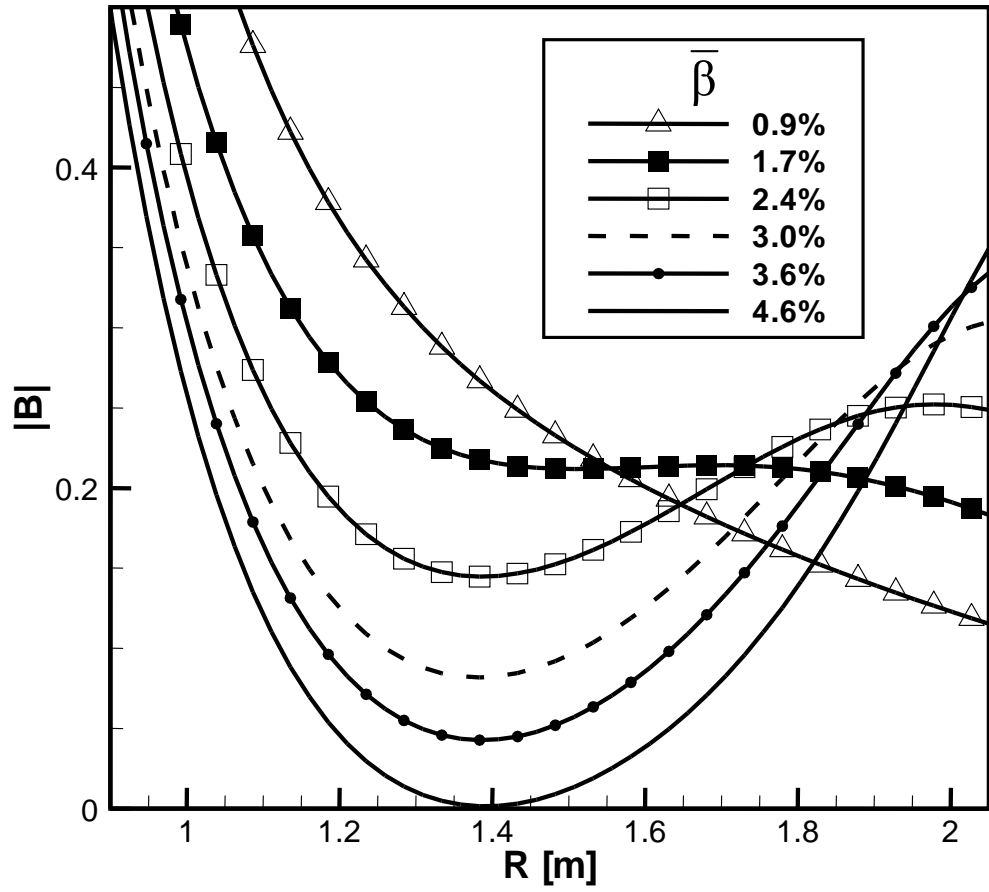Figure 3: LDX magnet schematic representation.

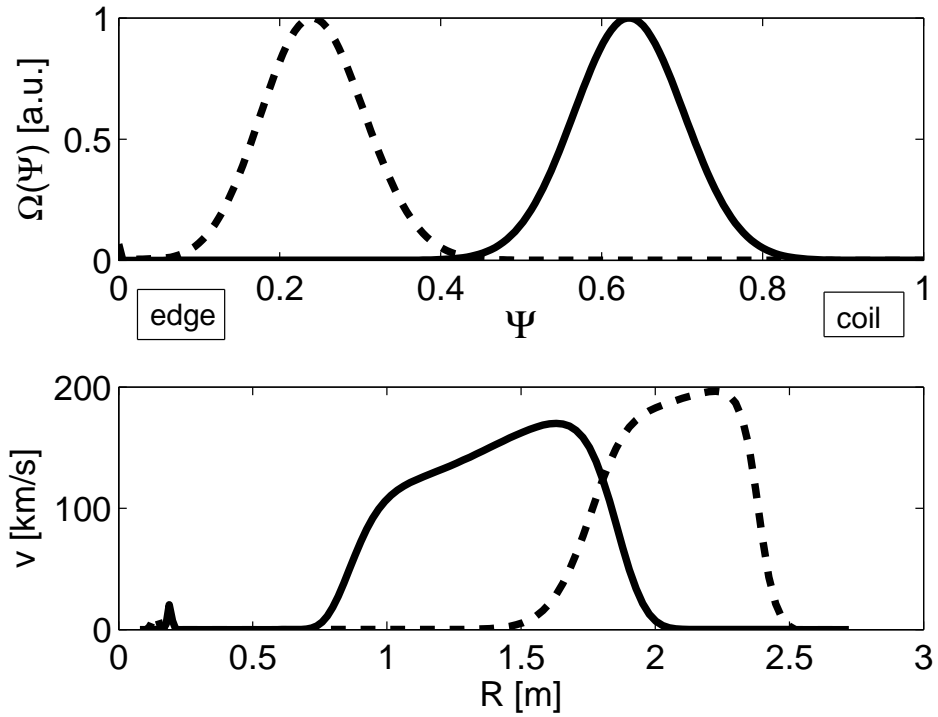Figure 4: Poloidal field in [T] along the midplane for increasing pressure values.

Figure 5: Top part: Toroidal rotation frequency $\Omega(\psi)$ (in arbitrary units) for the two flow profile cases. Edge-flow case is dashed, central-flow case is represented with a continuous line. Bottom part: Resulting velocity in [km/s] in two high-flow equilibria. The equilibrium limit is reached in the central-flow case (solid line), but not in the edge flow case (dashed line).
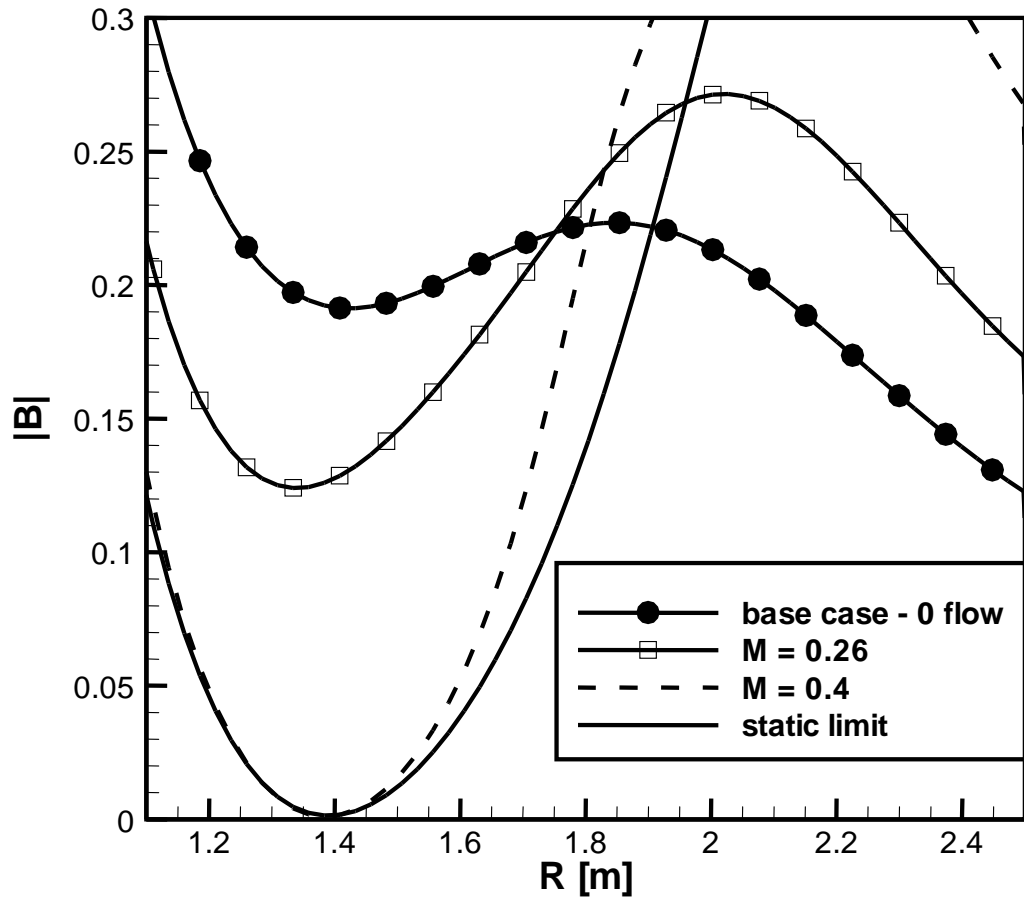
Figure 6: $|B|$ next to the minimum field in the presence of various levels of rotation next to the pressure peak. The static equilibrium limit is included for reference.
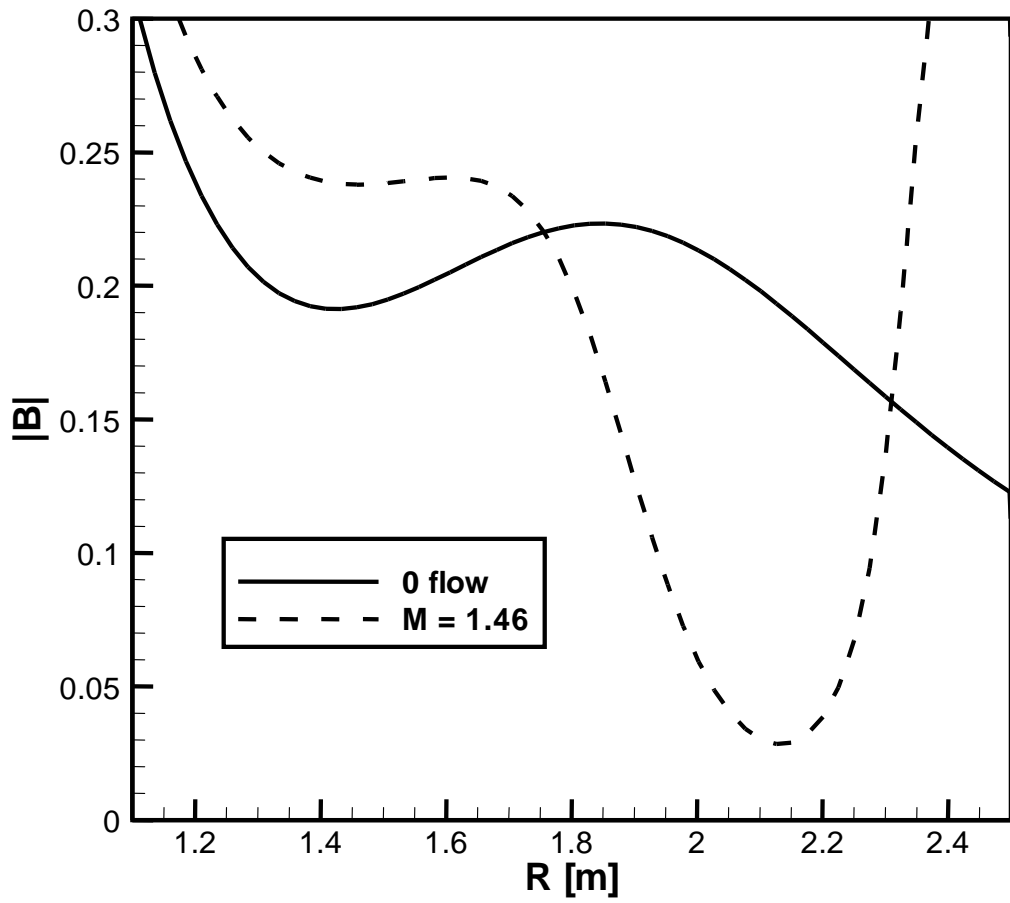
Figure 7: Poloidal field in [T] along the midplane for static and fast-flow equilibria.
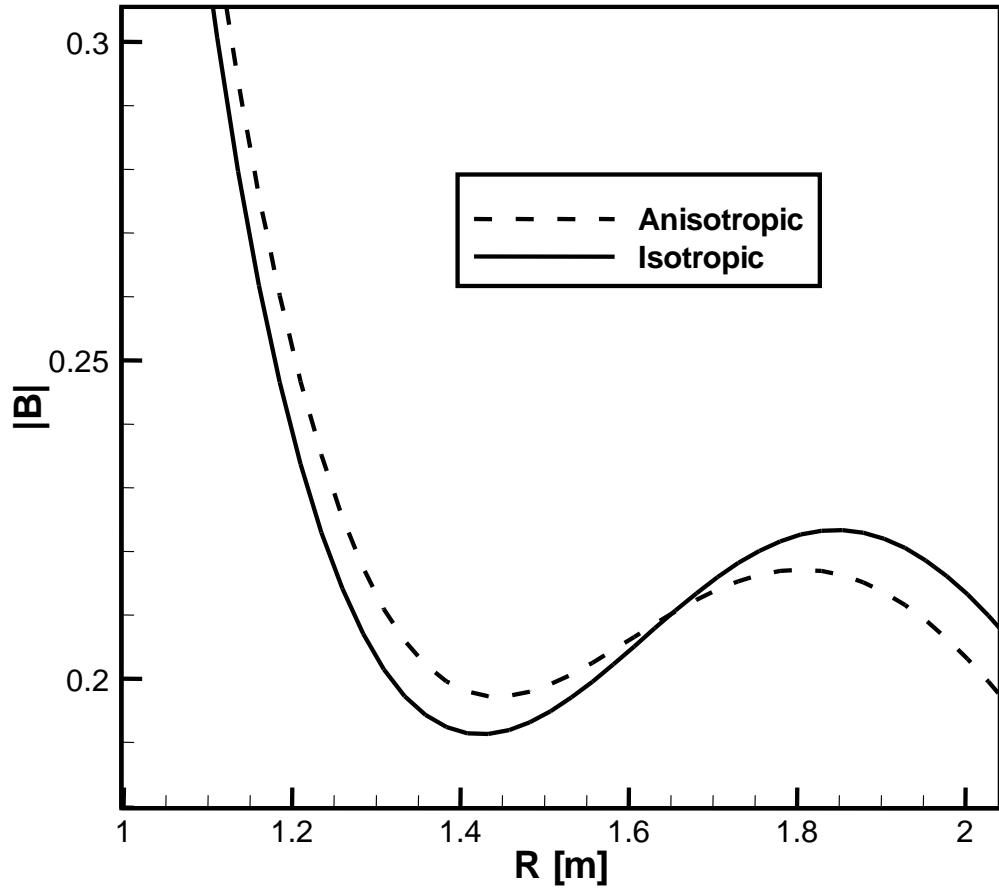
Figure 8: $|B|$ with $\bar{\beta} = 0.43\bar{\beta}_{max}$ for anisotropic (dashed line) and isotropic (solid line) equilibria.